ADVANCED OPTICAL MATERIALS
www.advopticalmat.de

High Speed and Stable Solution-Processed Triple Cation Perovskite Photodetectors

*Ting Zhang, Jiang Wu, Peng Zhang, Waseem Ahmad, Yafei Wang, Mahdi Alqahtani, Hao Chen, Chunming Gao, Zhi David Chen, Zhiming Wang, and Shibin Li**

Photodetectors, which can convert light signals into electrical signals, are important opto-electronic devices in imaging, optical communication, biomedical/biological sensing, and so on. Here a solution-processed photodetector based on the triple cation perovskite is demonstrated. The perovskite photodetectors show a high detectivity, high speed, as well as excellent environmental stability. Operating at a low voltage bias of 2 V, the photodetectors exhibit a large on/off ratio of 10^5, high specific detectivity of ≈10^{13} Jones, and a fast photoresponse with 3 dB bandwidth up to 0.82 MHz. Further analysis demonstrates that such performance originates from the modulated Schottky barrier height by illumination. The barrier suppresses dark current without any illumination, but it can be effectively lowered under illumination, thus resulting in a more efficient charge extraction and collection. The results demonstrate a great potential of triple cation perovskite in photodetection and provide a route to achieve high performance devices.

1. Introduction

Currently, commercial photodetectors (PDs) are mainly made from the inorganic semiconductor materials, including Si, ZnO, GaN, and InGaAs.[1–6] These devices show fast response and high responsivity due to their outstanding electrical and optical properties. However, such materials are either expensive or require vacuum equipment, e.g., metal-organic chemical vapor deposition, to fabricate,[7–9] which places a restriction on a wide deployment. In recent years, organometal trihalide perovskites (OTPs) (with a structure of ABX_3, where A is an organic cation $CH_3NH_3^+$ (MA), B is Pb^{2+}, X is a halide anion or mixed halide) have drawn great attention and been a very promising candidate for opto-electronic applications due to low cost and high throughput solution process. Since the discovery of perovskite-based solar cells (PSCs) by Miyasaka and co-workers[10] power conversion efficiencies have exceeded 22% in less than seven years,[11] thanks to the outstanding physics properties, including the low exciton binding energy, strong light absorption, long carrier lifetime, large carrier diffusion coefficient, and low charge recombination rate.[12–16] These features also make the emerging perovskite materials a promising alternative to conventional semiconductors used in PDs. Indeed, solution-processed OTPs have yielded PDs with excellent device performance.[16–24]

For instance, both polycrystalline films and single crystals of OTPs have been successfully used to fabricate the narrowband and broadband photodetectors.[25–27] As one of the earliest discovered and extensively researched perovskite materials, $MAPbI_3$ has been regarded as one of the most potential materials for PDs due to its broadband absorption and superb light sensitivity. Dong et al. reported a $MAPbI_3$-based photodetector with excellent photoconductive properties.[20] Su et al. reported a self-powered photodetector based on $MAPbI_3$, which exhibited excellent responsivity and rapid response time for wavelength ranging from ultraviolet to visible light.[28] Chen et al. fabricated a flexible UV–vis–NIR photodetector based on $MAPbI_3$ with excellent mechanical flexibility and durability.[18] However, some issues about this material still exist. $MAPbI_3$ tends to degrade and dissociate into MAI and PbI_2 in air.[29–31] Recent work on $FAPbX_3$ (FA: $CH_3(NH_2)_2^+$, X = I, Br, Cl) PSCs demonstrates better thermal durability than methylammonium perovskites.[31,32] However, $FAPbI_3$ has two different phases at room temperature: α-phase (desired perovskite phase) and δ-phase (photo-inactive phase). Also, the α-phase perovskite of $FAPbI_3$, which is sensitive to solvents and moisture, would turn into the undesired δ-phase in an air atmosphere.[33]

Dr. T. Zhang, Dr. P. Zhang, Dr. W. Ahmad, Dr. Y. Wang, Dr. H. Chen, Prof. C. Gao, Prof. S. Li
School of Optoelectronic Information
University of Electronic Science and Technology of China
Chengdu 610054, China
E-mail: shibinli@uestc.edu.cn
Dr. J. Wu, Dr. M. Alqahtani
Department of Electronic and Electrical Engineering
University College London
Torrington Place, London WC1E 7JE, UK
Dr. J. Wu, Prof. Z. Wang
Institute of Fundamental and Frontier Sciences
University of Electronic Science and Technology of China
Chengdu 610054, China
Prof. Z. D. Chen
Department of Electrical & Computer Engineering and Center for Nanoscale Science & Engineering
University of Kentucky
Lexington, Kentucky 40506, USA
The ORCID identification number(s) for the author(s) of this article can be found under https://doi.org/10.1002/adom.201701341.

DOI: 10.1002/adom.201701341

To date, the best PSCs use mixed cations and halides,[11,34–36] e.g., $(CsPbI_3)_{0.05}[(FAPbI_3)_{0.83}(MAPbBr_3)_{0.17}]_{0.95}$. Tri-cation (Cs/MA/FA) and dual-anion (Br/I) mixed perovskite films are more stabilized and less effected by environmental factors (such as heat, moisture, and solvents).[35] Motivated by the success of cesium-containing triple cation perovskites in PSCs, PDs based on the mixed cation perovskites are expected to outperform its conventional counterparts. Herein, we report on triple cation mixed perovskite PDs exhibiting a fast response, high detectivity, large photocurrent on/off ratio, and excellent stability. To the best of our knowledge, it is the first demonstration of the triple cation perovskite photodetectors. Due to the optimum bandgap and large absorption coefficient, $(CsPbI_3)_{0.05}[(FAPbI_3)_{0.83}(MAPbBr_3)_{0.17}]_{0.95}$ is particularly suitable for broadband photodetector in the UV and visible light ranges.

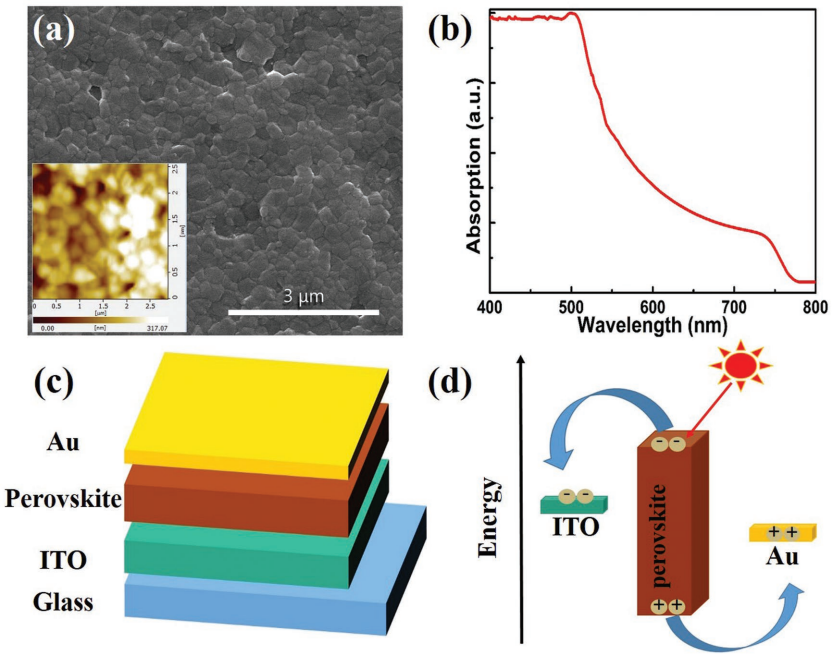

Figure 1. a) Top view SEM image and b) absorption spectra of the perovskite film. The inset AFM map in (a) show a RMS of 58 nm, demonstrating the smooth morphology on surface. c) Schematic of the triple cation mixed perovskite photodetector. d) Schematic diagram of charge carrier transfer in the device under illumination.

2. Results and Discussion

All fabrication details are given in the experimental methods section. **Figure 1**a,b shows the SEM image and the absorption spectrum of a perovskite film prepared on an indium tin oxide (ITO) substrate, respectively. The film, which is composed of uniform grains, is smooth and compact without any pinholes. The atomic force microscopy (AFM) picture, which shows a root mean square roughness (RMS) of 58 nm, further demonstrates the smooth surface morphology, as displayed in the inset of Figure 1a. The absorption spectrum covers a broad spectral region, 400–760 nm. It has a sharp absorption edge representing a bandgap of 1.63 eV. As schematically illustrated in Figure 1c, the device structure of the photodetectors is a stack of glass/ITO/perovskite/gold. When the device is illuminated from ITO side (bottom electrode), charge carriers generated by above-bandgap photons at the interface between perovskite film and ITO drift across the compact film under bias voltages; the electrons drift towards the ITO and the holes to the Au. Both types of carriers will be collected finally to form the output photocurrent, as shown in Figure 1d.

To investigate whether Cs enhances the thermal stability of mixed perovskite, we measured and compared the absorption of as-prepared perovskite samples that were kept in different conditions. As shown in **Figure 2**a, it is evident that the absorption of perovskite films without Cs decreases quickly after being treated by successive thermal stress. The surface degrades visibly than before (see Figure S1 in the Supporting Information). Contrarily, the triple cation mixed perovskite film remains the black color and good absorption. The X-ray

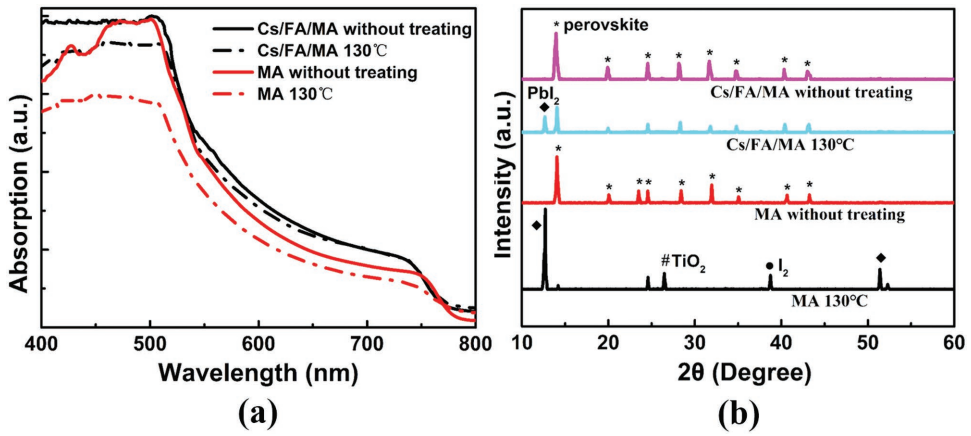

Figure 2. a) Optical absorption and b) XRD data of triple cation mixed perovskite and $MAPbI_3$. The treating process means perovskite films were annealed at 130 °C for 3 h in dry air.

diffraction (XRD) data in Figure 2b demonstrates that the MA cation perovskite material decomposed and generated PbI_2 after heating for 3 h, resulting in a distinct change in perovskite diffraction peak. However, the diffraction peak value of the triple cation perovskite film did not decrease much after being treated by successive thermal stress for 3 h. The results exhibit that the Cs-containing perovskite films are more stable and can suppress the decomposition of $MAPbI_3$ effectively.

Figure 3 shows the device characteristics of the photodetectors. The *I–V* curves were obtained under dark and light illumination conditions. It is evident that the photocurrent curve shows a rectification behavior, which indicates that a junction barrier exists between the ITO and perovskite films. Such a junction barrier may be attributed to a Schottky contact formed at the ITO/perovskite interface and the surface states (including surface defects, vacancies, and absorption).[37] Schottky junctions are formed at the interface between many semiconductors and metals. A high work function of a metal is considered to be favored for constructing Schottky junctions when it contacts with perovskites.[38] Biased at 2 V, the device showed a dark current as low as 1.5 nA, and the photocurrent increased to 3.9 μA with the illumination intensity of 0.05 mW cm^{-2} using a 635 nm laser diode (LD) light source (see Figure 3a,b). The high photocurrent gives a high on/off ratio (rectification ratio) larger than 10^3 under a bias of 2 V. To further test the photoresponse behavior of the photodetector, photocurrents were measured under different incident light intensities ranging from 0.05 to 3.5 mW cm^{-2}, as shown in Figure 3c. Photocurrent increases linearly with the increasing incident light intensity, indicating low recombination loss of photogenerated carries in the device. Upon light irradiation, the photocurrent increased sharply, and then decreased rapidly when the light was turned off. Figure S2 (Supporting Information) shows that the device exhibits a reproducible photocurrent response to periodic on/off light after being exposed to light illumination over 2000 s. With a high power irradiation of 3.5 mW cm^{-2}, the light-switching on/off ratio can be as high as 10^5 while the photocurrent reaches around 140 μA at a bias of 2 V. The results demonstrate high photosensitivity and capability of detecting light signal of low intensity.

Figure 3d shows the external quantum efficiency (EQE) spectra at different biases. The EQE value increased with increasing bias and can reach up to 300% measured at a bias of 10 V, due to the fact that excess charges were injected by the electrodes under applied bias voltages, except for the photogenerated charges. Moreover, the EQE curves agree well with the absorption curve (shown in Figure 1b). Specific responsivity was calculated and plotted in Figure 3e. It is observed that the responsivity monotonously increases with the increasing applied bias. With the applied bias voltages at 6 V, the EQE values exceed 100%, and the corresponding responsivities are superior to Si PD (<0.2 A/W) even at ultraviolet wavelength regions.[39] As a result, we obtained a higher responsivity of 1.63 A/W at a bias of 10 V for our device.

To further characterize the performance of PDs, specific detectivity (D^*) is analyzed. Assuming dark current is the main contribution to the total noise, D^* can be expressed as $D^* = \frac{R}{\sqrt{(2qJ_d)}}$, where J_d is the dark current density. Figure 3f shows the detectivity curves measured at different bias. D^* under −1 and −2 V were calculated to be above 10^{12} and 10^{13} Jones (Jones = cm × $Hz^{\frac{1}{2}}$ × W^{-1}), respectively. The high detectivity value means that weak light signals can be detected and

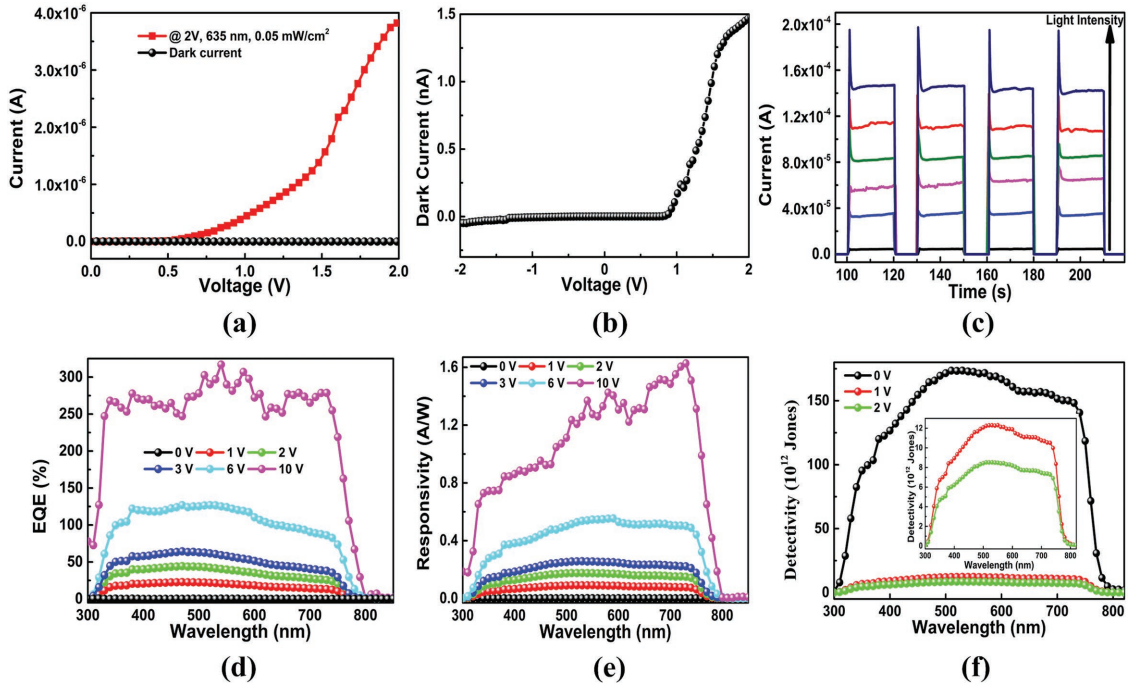

Figure 3. a) *I–V* curves of the device in the dark and under illumination with light intensity of 0.05 mW cm^{-2} (635 nm light source) at 2 V. b) Zoomed-up dark current curve. c) *I–t* curves of the PD under bias voltage of 2 V at different light intensities (635 nm light source). d) EQE and e) responsivity spectra under different biases. f) Specific detectivities of our photodetector under different biases. The insert is an enlarged portion of D^* at −1 and −2 V.

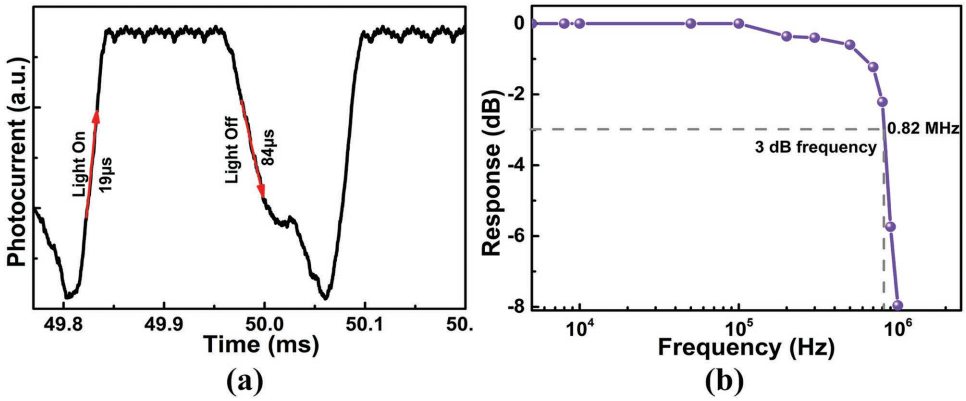

Figure 4. a) Transient photocurrent response of our detector at a frequency of 20 kHz. b) Normalized photoresponse as a function of light frequency, showing a 3 dB bandwidth of 0.82 MHz.

transferred into large electrical signals. At 0 V, D^* is measured as high as 10^{14} Jones. A smaller J_d mainly ascribes to the low thermal emission rates and high perovskite film quality, both of which prevent large leakage current. Noise current, a key figure of merit for photodetectors, is directly measured using a lock-in amplifier. The measured spectrum, shown in Figure S4 in the Supporting Information, further demonstrated that the trip-cation perovskite PDs possess a small noise current (<1 pA/Hz$^{1/2}$), which is about one order of magnitude lower than that of a referred Si PD.[40]

Another important figure of merit for photodetectors is the response speed, which can be defined as the rising time of the photocurrent from 10% of the maximum to 90%, or vice versa. We used an oscilloscope to record the temporal response. In **Figure 4**a, the rise time and decay time for our device are extracted to be 19 and 84 μs, respectively. The fast response time is primarily determined by the charge transport and collection, which would be strongly affected by the electronic trap states existing at the interface of semiconductor/metal. It is observed that the decay time shows a slower decay rate. An interpretation for such a phenomenon is possible presence of surface states which keep photocarriers from immediate collection or recombination after switching off illumination.[19] Finally, we measured the response of our detector to a pulsed LD light at different frequencies. Figure 4b depicts the curve of normalized response versus light pulse frequency, showing the −3 dB bandwidth (f_{-3dB}) is 0.82 MHz. The bandwidth is larger than that of the reported photodetectors based on a bulk perovskite single crystal and perovskite nanowires.[24,27] To compare the device reported in this work to the state-of-the-arts, the performance of perovskite-based photodetectors are briefly summarized in **Table 1**. In comparison with the previous works, the simple photodetector demonstrated excellent performance in all aspects, including EQE (317%), responsivity (1.63 A/W), detectivity (>10^{13} Jones), and rise/decay time (1.9×10^{-5}/8.4×10^{-5} s).

The energy band diagram (see in **Figure 5**) of our device under dark and illumination conditions was plotted to gain an insight into the high device performance. Although the energy level diagram of $(CsPbI_3)_{0.05}[(FAPbI_3)_{0.83}(MAPbBr_3)_{0.17}]_{0.95}$ has never been pictured in the past, an approximate energy positions of valence and conduction bands for the triple cation perovskite can be estimated using the energy levels of three different perovskites,[51,52] as shown in Figure 5a. Considering the optical absorption band edge, we estimated the conduction band minimum of triple cation perovskite should be much higher than that of $FAPbI_3$, and the valence band maximum of triple cation perovskite is slightly higher than that of $FAPbI_3$, as shown in Figure 5b. However, the work function of perovskite is sensitive to the synthesis conditions and defects in bulk materials due to ion redistribution.[53] The issue of ion-redistribution-based perovskite bulk transport is complicated. As being unambiguously studied in ref. [53] the process of ion redistribution, could be affected by a biased voltage and occur in the whole perovskite layer. Here, we focus our discussion on a simplified ion dynamics to describe the process. Under zero bias voltage and no illumination, the device is in an equilibrium state and the band alignment is shown in Figure 5c, of which ϕ_B means the Schottky barrier height. Specifically, due to charge transfer after bringing the ITO electrode in contact with the perovskite film, a depletion layer would be formed near the surface of perovskite film. As a result of the band bending, a Schottky barrier is formed at the ITO/perovskite interface. Both the depletion layer and the space charge region have been proved to be helpful in separating photoexcited charge carriers. When the device is under bias voltages and illumination, as shown in Figure 5d, the strong local electric field acting on Schottky barrier area will separate the photogenerated holes and electrons quickly and reduce the hole–electron recombination rate, leading to an increase of free carrier density. The increased free carrier density would lower the effective Schottky barrier height by changing the Femi level, thus resulting in the easier tunneling and transport for carriers. In other words, photogenerated electrons would inject into the ITO electrode and the holes would move to the gold contact, as schematically depicted in Figure 5d and Figure 1d. Once the light illumination is turned off, the carrier recombination will increase quickly that reduce the free carrier density greatly, resulting in a significantly increased Schottky barrier height.

To check the environmental stability of our photodetector, we measured the photocurrent response of a device upon illumination with a 635 nm light (0.05 mW cm^{-2}) after being stored for one week in ambient conditions with 35–45% relative

Table 1. Performance comparison of our photodetector with other reported photodetectors based on perovskites.

Materials structure	Configurations	EQE [%]	Responsivity [A/W]	Detectivity [Jones]	Rise/decay time [ms]	Refs.
Triple cation mixed perovskite film	Photoconduction	317	1.63	$\approx 10^{13}$	0.019/0.084	Our work
$MAPbI_3$ film	Photoconduction	1190	3.49	–	≈100/100	[21]
$MAPbI_3$ network	Photoconduction	–	0.1	1.02×10^{12}	0.3/0.4	[41]
$MAPbI_3$ island	Photoconduction	–	–	–	≈40/50	[42]
$MAPbI_3$ NW arrays	Photoconduction	–	12 500	1.73×10^{11}	0.00034/0.00042	[24]
$MAPbI_3$ NW arrays	Photoconduction	–	1.3	2.5×10^{12}	0.2/0.3	[43]
$MAPbI_3$ crystal	Photoconduction	2×10^5	1604	$\approx 10^{13}$	≈0.03/0.02	[26]
$MAPbI_3$+PDPP3T film	Photoconduction	≈10	0.05	8.8×10^{10}	40/140	[18]
$MAPbI_3$+WS_2 film	Photoconduction	–	17	2×10^{12}	2.7/7.5	[44]
$CsPbBr_3$ nanosheets	Photoconduction	54	0.64	–	0.019/0.024	[45]
$MAPbI_3$ film	Photodiode	–	14.5	–	0.0002/0.0007	[9]
$MAPbI_3$_xClx film	Photodiode	80	–	$\approx 10^{14}$	1.6×10^{-4}	[25]
$MAPbBr_3$ crystal	Photodiode	–	4000	$>10^{13}$	–/0.025	[46]
$MAPbI_3$+PDPPTDTPT film	Photodiode	≈75	–	$>10^{11}$	5×10^{-6}	[47]
$MAPbI_3$ film	Phototransistor	≈80	320	–	0.0065/0.005	[48]
$MAPbI_3$+graphene film	Phototransistor	5×10^4	180	$>10^9$	87/540	[49]
$MAPbI_3$+MoS_2 film	Phototransistor	–	1.94×10^6	1.29×10^{12}	6170/4500	[50]

humidity (see Figure S3, Supporting Information). Notably, our device showed nearly consistent photocurrent response, indicating good environmental stability. In comparison, the responsivity of a $MAPbI_3$-based photodetector stored under the same conditions decreased rapidly and significantly and after one day, no obvious photocurrent can be detected.[18]

Figure 6 shows the triple-cation perovskite device characteristics after being stored for two months in ambient

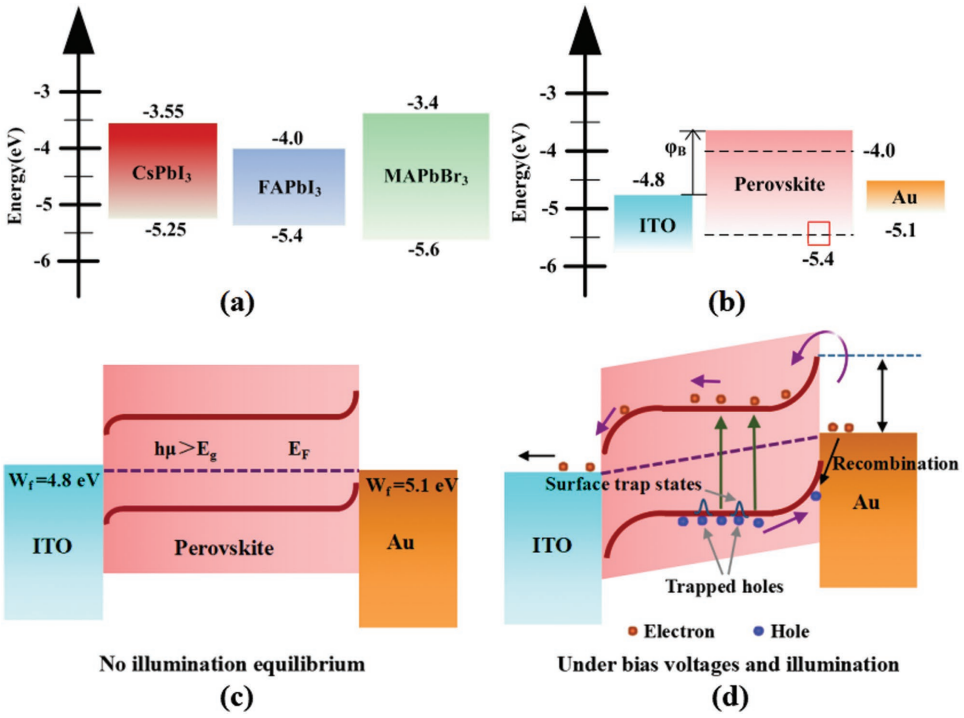

Figure 5. a) Band diagram of $CsPbI_3$, $FAPbI_3$, $MAPbBr_3$. b) Band diagram for the triple cation perovskite device. Schematic illustrations of band structure for our device c) under zero bias voltage in the dark and d) under bias voltages and illumination. Upon illumination, the lower Schottky barrier height leads to photogenerated holes move to the surface and are trapped by the surface trap states, leaving behind more unpaired electrons move to the electrode, resulting in a great increase of photocurrent and photoresponse.

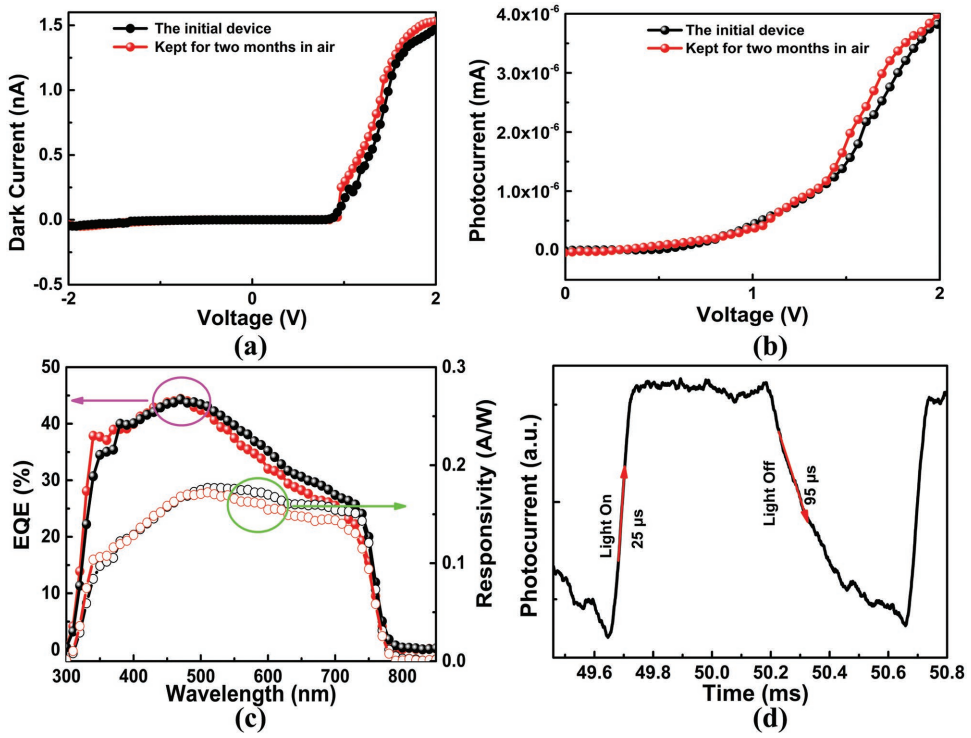

Figure 6. Opto-electronic performance of our photodetectors kept for two months in ambient air. *I–V* curves of the device a) in the dark and b) under illumination with light intensity of 0.05 mW cm^{-2} (635 nm light source) at 2 V. c) EQE and responsivities spectra biased at 2 V. Black represents EQE and responsivity of the initial device. Red means these parameters of the device measured after keeping for two months in ambient air. d) Transient photocurrent response of our detector at a frequency of 5 kHz.

conditions with 35–45% relative humidity. To compare and evaluate a device lifetime, the measurement is under the same conditions as before (illuminated with a 0.05 mW cm^{-2} 635 nm light and biased at 2 V). Comparing the curves of dark current, photocurrent, EQE and responsivity, a negligible change is observed after being stored for two months under the above-mentioned conditions. In Figures S5 and S6 in the Supporting Information, we further measured the photocurrent of a device after being stored for two months. Apparently, our device showed nearly consistent photocurrent response, indicating good stability. The small changes presented in the figure could be resulted from experimental run-to-run errors. Additionally, we compare the optical photos and absorption curves of the as-prepared device and aged device (shown in Figure S7, Supporting Information), confirming a good stability. Figure 6d depicts the rise and decay time for our device kept for two months. The extracted values are 25 and 95 µs, respectively, which are slightly larger than the response time of initial device but remain the same order of magnitude. Therefore, the triple cation perovskite-based photodetectors can resist humidity penetration and oxygen degradation effectively, as evidenced from the consistent device performance after being used and kept in ambient air for extended time.

3. Conclusion

In summary, we present triple cation perovskite-based photodetectors that can be applied to broadband spectrum detection in this work. The device with a simple configuration shows excellent performance, which is comparable to or even better than $MAPbI_3$-based photodetectors. Operating at a bias of 2 V, the as-prepared photodetectors exhibited a large light on/off ratio of 10^5 upon illumination with 635 nm light, high specific detectivity (≈10^{13} Jones), 3 dB bandwidth (0.82 MHz), as well as good environmental stability (>2 months). Such an excellent photoresponse property is related to the Schottky barrier formed by the contact of ITO/perovskite; it would be effectively lower when illuminated, thus resulting in more efficient charge extraction and collection. This work demonstrates a great potential of triple cation perovskite in opto-electronic detection, and provides a promising route to achieve high performance.

4. Experimental Section

Synthesis and Characterization of Triple Cation Perovskite: ITO substrates were cleaned by acetone, ethyl alcohol and deionized water with each step for 15 min. After that, the substrates were further treated by UV ozone. The mixed perovskite precursor solutions were prepared by mixing 1 M (mol L^{-1}) $CH_3(NH_2)_2I$ (FAI), 1.1 M PbI_2, 0.2 M MABr, and 0.2 M $PbBr_2$ in anhydrous *N*,*N*-dimethylformamide (DMF):dimethyl sulfoxide (DMSO) (4:1 v/v). After stirring for 12 h, 1.5 M CsI (predissolved in DMSO) was add into the mixed perovskite solutions with a volume ratio of 5:95 to obtain the desired composition of triple cation perovskite. All the early-stage preparations were carried in a nitride-filled glove box. The morphologies of as-prepared films were measured by field emission scanning electron microscopy. AFM images were measured by 300HV scanning force microscope (SEIKO) to illustrate the surface morphology of films. XRD patterns were recorded using an X-ray diffractometer

(Cu Kα radiation, λ = 1.54056 Å) to study the crystal quality of the perovskite films. The UV–vis absorption spectra were measured using a UV–vis spectrophotometer (Shimadzu UV-3101 PC).

Fabrication of the Photodetectors: The precursor solution was spin coated by two-steps: 1000 and 5000 rpm for 10 and 40 s, respectively. At the last 5 s of the coating, 200 µL of chlorobenzene was added to the substrate. Films turned dark immediately after this treatment. The substrates were then annealed at 100 °C for 1 h in a nitrogen-filled glovebox. Finally, gold electrodes with a thickness of 80 nm as the back contact were deposited by thermal evaporation. For each device, the photoactive area defined by the electrode was 0.04 cm^2.

Photoresponse Measurements: The typical current–voltage characteristics of the devices were measured using a Keithley 4200 Semiconductor Parametric Analyzer under the illumination of a 635 nm LD light. Photocurrent with on/off cycles was measured with an oscilloscope (Agilent DOS5012A) and an optical chopper modulating the light illuminated on the device. External quantum efficiencies and responsivities were characterized by a QE-R measurement system equipped with a calibrated Si PD as the reference (Enli tech from Taiwan). Noise current was directly measured using a SR830 lock-in amplifier. The photodetectors were kept in a dark room during the measurements. All the measurements were performed at room temperature in the ambient atmosphere.

Supporting Information

Supporting Information is available from the Wiley Online Library or from the author.

Acknowledgements

This work was supported by National Natural Science Foundation of China under Grant Nos. 61421002, 61474015, 61574029, 61471085, and 61371046. This work was also partially supported by University of Kentucky.

Conflict of Interest

The authors declare no conflict of interest.

Keywords

environmental stability, photoresponse properties, Schottky barrier, triple cation perovskite photodetectors

Received: December 10, 2017
Revised: March 16, 2018
Published online:

[1] L. Wang, J. Jie, Z. Shao, Q. Zhang, X. Zhang, Y. Wang, Z. Sun, S.-T. Lee, *Adv. Funct. Mater.* **2015**, *25*, 2910.
[2] M. Otto, M. Algasinger, H. Branz, B. Gesemann, T. Gimpel, K. Füchsel, T. Käsebier, S. Kontermann, S. Koynov, X. Li, V. Naumann, J. Oh, A. N. Sprafke, J. Ziegler, M. Zilk, R. B. Wehrspohn, *Adv. Opt. Mater.* **2015**, *3*, 147.
[3] T. Zhang, B. Liu, W. Ahmad, Y. Xuan, X. Ying, Z. Liu, Z. Chen, S. Li, *Nanoscale Res. Lett.* **2017**, *12*, 522.
[4] Y. Jin, J. Wang, B. Sun, J. C. Blakesley, N. C. Greenham, *Nano Lett.* **2008**, *8*, 1649.
[5] D. Fan, K. Lee, S. R. Forrest, *ACS Photonics* **2016**, *3*, 670.
[6] X. Wang, J. Song, P. Li, J. H. Ryou, R. D. Dupuis, C. J. Summers, Z. L. Wang, *J. Am. Chem. Soc.* **2005**, *127*, 7920.
[7] X. Gong, M. Tong, Y. Xia, W. Cai, J. S. Moon, Y. Cao, G. Yu, C.-L. Shieh, B. Nilsson, A. J. Heeger, *Science* **2009**, *325*, 1665.
[8] K.-J. Baeg, M. Binda, D. Natali, M. Caironi, Y.-Y. Noh, *Adv. Mater.* **2013**, *25*, 4267.
[9] Y. Guo, C. Liu, H. Tanaka, E. Nakamura. *J. Phys. Chem. Lett.* **2015**, *6*, 535.
[10] A. Kojima, K. Teshima, Y. Shirai, T. Miyasaka, *J. Am. Chem. Soc.* **2009**, *131*, 6050.
[11] W. S. Yang, B. W. Park, E. H. Jung, N. J. Jeon, Y. C. Kim, D. U. Lee, S. S. Shin, J. Seo, E. K. Kim, J. H. Noh, S. I. Seok, *Science* **2017**, *356*, 1376.
[12] T. Leijtens, S. D. Stranks, G. E. Eperon, R. Lindblad, E. M. J. Johansson, I. J. McPherson, H. Rensmo, J. M. Ball, M. M. Lee, H. J. Snaith, *ACS Nano* **2014**, *8*, 7147.
[13] X. Gu, Y. Wang, T. Zhang, D. Liu, R. Zhang, P. Zhang, J. Wu, Z. D. Chen, S. Li, *J. Mater. Chem. C* **2017**, *5*, 10754.
[14] S. Li, P. Zhang, Y. Wang, H. Sarvari, D. Liu, J. Wu, Y. Yang, Z. Wang, Z. D. Chen, *Nano Res.* **2017**, *10*, 1092.
[15] D. Liu, S. Li, P. Zhang, Y. Wang, R. Zhang, H. Sarvari, F. Wang, J. Wu, Z. Wang, Z. D. Chen, *Nano Energy* **2017**, *31*, 462.
[16] M. I. Saidaminov, M. A. Haque, J. Almutlaq, S. Sarmah, X.-H. Miao, R. Begum, A. A. Zhumekenov, I. Dursun, N. Cho, B. Murali, O. F. Mohammed, T. Wu, O. M. Bakr, *Adv. Opt. Mater.* **2017**, *5*, 1600704.
[17] H. Wang, D. H. Kim, *Chem. Soc. Rev.* **2017**, *46*, 5204.
[18] S. Chen, C. Teng, M. Zhang, Y. Li, D. Xie, G. Shi, *Adv. Mater.* **2016**, *28*, 5969.
[19] V. Adinolfi, O. Ouellette, M. I. Saidaminov, G. Walters, A. L. Abdelhady, O. M. Bakr, E. H. Sargent, *Adv. Mater.* **2016**, *28*, 7264.
[20] R. Dong, Y. Fang, J. Chae, J. Dai, Z. Xiao, Q. Dong, Y. Yuan, A. Centrone, X. C. Zeng, J. Huang, *Adv. Mater.* **2015**, *27*, 1912
[21] X. Hu, X. Zhang, L. Liang, J. Bao, S. Li, W. Yang, Y. Xie, *Adv. Funct. Mater.* **2014**, *24*, 7373.
[22] Y. Wang, Y. Zhang, Y. Lu, W. Xu, H. Mu, C. Chen, H. Qiao, J. Song, S. Li, B. Sun, Y.-B. Cheng, Q. Bao, *Adv. Opt. Mater.* **2015**, *3*, 1389.
[23] X. Li, D. Yu, J. Chen, Y. Wang, F. Cao, Y. Wei, Y. Wu, L. Wang, Y. Zhu, Z. Sun, J. Ji, Y. Shen, H. Sun, H. Zeng, *ACS Nano* **2017**, *11*, 2015.
[24] W. Deng, L. Huang, X. Xu, X. Zhang, X. Jin, S.-T. Lee, J. Jie, *Nano Lett.* **2017**, *17*, 2482.
[25] L. Dou, Y. M. Yang, J. You, Z. Hong, W.-H. Chang, G. Li, Y. Yang, *Nat. Commun.* **2014**, *5*, 5404.
[26] M. I. Saidaminov, M. A. Haque, M. Savoie, A. L. Abdelhady, N. Cho, I. Dursun, U. Buttner, E. Alarousu, T. Wu, O. M. Bakr, *Adv. Mater.* **2016**, *28*, 8144.
[27] Y. Fang, Q. Dong, Y. Shao, Y. Yuan, J. Huang, *Nat. Photonics* **2015**, *9*, 679.
[28] L. Su, Z. X. Zhao, H. Y. Li, J. Yuan, Z. L. Wang, G. Z. Cao, G. Zhu, *ACS Nano* **2015**, *9*, 11310.
[29] Y. Han, S. Meyer, Y. Dkhissi, K. Weber, J. M. Pringle, U. Bach, L. Spiccia, Y.-B. Cheng, *J. Mater. Chem. A* **2015**, *3*, 8139.
[30] P. Zhang, J. Wu, Y. Wang, H. Sarvari, D. Liu, Z. D. Chen, S. Li, *J. Mater. Chem. A* **2017**, *5*, 17368.
[31] G. E. Eperon, S. D. Stranks, C. Menelaou, M. B. Johnston, L. M. Herz, H. J. Snaith. *Energy Environ. Sci.* **2014**, *7*, 982.
[32] J.-W. Lee, D.-H. Kim, H.-S. Kim, S.-W. Seo, S. M. Cho, N.-G. Park, *Adv. Energy Mater.* **2015**, *5*, 1501310.
[33] C. Yi, J. Luo, S. Meloni, A. Boziki, N. Ashari-Astani, C. Grätzel, S. M. Zakeeruddin, U. Röthlisberger, M. Grätzel, *Energy Environ. Sci.* **2016**, *9*, 656.
[34] Y. Wang, J. Wu, P. Zhang, D. Liu, T. Zhang, L. Ji, X. Gu, Z. D. Chen, S. Li, *Nano Energy* **2017**, *39*, 616.

[35] M. Saliba, T. Matsui, J.-Y. Seo, K. Domanski, J.-P. Correa-Baena, M. K. Nazeeruddin, S. M. Zakeeruddin, W. Tress, A. Abate, A. Hagfeldt, M. Grätzel, *Energy Environ. Sci.* **2016**, *9*, 1989.
[36] T. Ye, S. Ma, X. Jiang, L. Wei, C. Vijila, S. Ramakrishna, *Adv. Funct. Mater.* **2017**, *27*, 1606545.
[37] H. Kind, H. Yan, B. Messer, M. Law, P. Yang, *Adv. Mater.* **2002**, *14*, 158.
[38] P. A. Shaikh, D. Shi, J. R. D. Retamal, A. D. Sheikh, M. A. Haque, C.-F. Kang, J.-H. He, O. M. Bakr, T. Wu, *J. Mater. Chem. C* **2016**, *4*, 8304.
[39] F. Guo, B. Yang, Y. Yuan, Z. Xiao, Q. Dong, Y. Bi, J. Huang, *Nat. Nanotechnol.* **2012**, *7*, 798.
[40] S. Malik, A. K. Ray, S. Bruce, *Semicond. Sci. Technol.* **2005**, *20*, 453.
[41] H. Deng, X. Yang, D. Dong, B. Li, D. Yang, S. Yuan, K. Qiao, Y.-B. Cheng, J. Tang, H. Song, *Nano Lett.* **2015**, *15*, 7963.
[42] Y. Zhang, J. Du, X. Wu, G. Zhang, Y. Chu, D. Liu, Y. Zhao, Z. Liang, J. Huang, *ACS Appl. Mater. Interfaces* **2015**, *7*, 21634.
[43] H. Deng, D. Dong, K. Qiao, L. Bu, B. Li, D. Yang, H.-E. Wang, Y. Cheng, Z. Zhao, J. Tang, H. Song, *Nanoscale* **2015**, *7*, 4163.
[44] C. Ma, Y. Shi, W. Hu, M.-H. Chiu, Z. Liu, A. Bera, F. Li, H. Wang, L.-J. Li, T. Wu, *Adv. Mater.* **2016**, *28*, 3683.
[45] J. Song, L. Xu, J. Li, J. Xue, Y. Dong, X. Li, H. Zeng, *Adv. Mater.* **2016**, *28*, 4861.
[46] M. I. Saidaminov, V. Adinolfi, R. Comin, A. L. Abdelhady, W. Peng, I. Dursun, M. Yuan, S. Hoogland, E. H. Sargent, O. M. Bakr, *Nat. Commun.* **2015**, *6*, 8724.
[47] L. Shen, Y. Lin, C. Bao, Y. Bai, Y. Deng, M. Wang, T. Li, Y. Lu, A. Gruverman, W. Li, J. Huang, *Mater. Horiz.* **2017**, *4*, 242.
[48] F. Li, C. Ma, H. Wang, W. Hu, W. Yu, A. D. Sheikh, T. Wu, *Nat. Commun.* **2015**, *6*, 8238.
[49] Y. Lee, J. Kwon, E. Hwang, C.-H. Ra, W. J. Yoo, J.-H. Ahn, J. H. Park, J. H. Cho, *Adv. Mater.* **2015**, *27*, 41.
[50] D.-H. Kang, S. R. Pae, J. Shim, G. Yoo, J. Jeon, J. W. Leem, J. S. Yu, S. Lee, B. Shin, J.-H. Park, *Adv. Mater.* **2016**, *28*, 7799.
[51] C.-C. Chueh, C.-Z. Li, A. K.-Y. Jen, *Energy Environ. Sci.* **2015**, *8*, 1160.
[52] Y. G. Kim, T.-Y. Kim, J. H. Oh, K. S. Choi, Y.-J. Kim, S. Y. Kim, *Phys. Chem. Chem. Phys.* **2017**, *19*, 6257.
[53] X. Guan, W. Hu, M. A. Haque, N. Wei, Z. Liu, A. Chen, T. Wu, *Adv. Funct. Mater.* **2018**, *28*, 1704665.